Error Analysis and the Development of an Error Mitigation Approach for Use in the Rotation Fiber Optic Gyro Inertial Navigation System

Zhao Qi, Qiuying Wang

Abstract—The fiber optic gyro (FOG) inertial navigation system (INS) outputs its own absolute position containing an error that increases with time caused by the FOG error. According to our method, the INS was placed on a turntable with the assumption that the INS is typically fixed inside an autonomous underwater vehicle (AUV). Then, the INS was rotated on the turntable around one rotational axis according to specified rules. Consequently, the INS position error was decreased by the rotational motion. However, the INS attitude error was increased by the rotational motion. During rotation, a new type of concussion error was developed and added to the attitude error; the new error was found to be related to the rotational period. A method for error mitigation based on adjustments in the navigational parameters is proposed that is capable of rejecting the concussion error related to the rotational angular velocity, which then improves the attitude precision. The experiment was conducted with a FOG INS that was developed in our lab, and the results demonstrate that attitude error is inhibited by the introduction of the navigational parameters in the calculation process.

Index Terms—Rotation FOG INS, inertial measurement unit error, attitude error, navigation parameters, error mitigation

I. Introduction

THE typical autonomous underwater vehicle (AUV) is equipped with a fiber optic gyro (FOG) inertial navigation system (INS), allowing the vehicle to determine its own position and attitude in real time while it cruises without communication with the external environment, such as that provided by a support ship or GPS [1-3].

In a FOG INS, the transformation matrix from the body frame to the navigation frame is obtained using the angular velocity measured by the FOG [4-6]. Then, the acceleration in the navigation frame is calculated using the product of the transformation matrix and the acceleration measured by the accelerometer along the body frame [7-10]. Upon integrating the acceleration along the navigation coordinate system, the velocity of the vehicle is obtained; similarly, following a double integration of the acceleration along the navigation cordinate system, the position of the vehicle is obtained.

Zhao Qi is with College of Automation, Harbin Engineering University, Harbin, 150001, China (Corresponding author phone: +8613936138022; fax: +86-0451-82518741; e-mail: xuelang0106@163.com).

Qiuying Wang is with College of Automation, Harbin Engineering University, Harbin, 150001, China (e-mail: wqy869087@163.com).

Additionally, the attitude is calculated using the transformation matrix [11-14]. However, the INS outputs its own absolute position, containing an error that increases with time that is caused by the FOG error.

The approach of rotating the inertial measure unit (IMU) has attracted widespread attention [15]. The IMU is placed on a turntable with the assumption that it is fixed inside the AUV [16-19]. Then, the IMU is rotated on the turntable around one rotation axis according to established rules. Accordingly, the IMU error along the navigation coordinate system becomes a periodic quantity, eliminating the effect of the IMU error on the position accuracy [20-23].

Although the divergent position error can be decreased using the rotating technology, a new type of concussion error that is related to the rotational period is introduced to the attitude error. According to this problem, a method for error mitigation based on adjustments in the navigational parameters is proposed.

The paper is organized as follows: we provide the system principle of the FOG INS is provided in Section 2, and the relationship between the FOG error and the system misalignment is discussed. The attitude error formed during the rotational process is demonstrated in Section 3. The method for eliminating the attitude error based on adjustments in the navigational parameters is presented in Section 4. Section 5 presents the simulation and experimental results, followed by a presentation of the conclusions from Section 3 and Section 4.

II. The principle of FOG INS rotation

To make the problem realistically pertinent, a single-axis rotation rule is considered as the example for the navigation error analysis. The IMU is rotated along the oz-axis by rotational motion, and the navigation algorithm for the FOG INS rotation is shown in Fig. 1.

In Fig. 1, b represents the body coordinate system, n represents the navigational coordinate system, and s represents the IMU coordinate system.

Based on the basic assumptions that the frame and the frame exist in coincident coordinate systems, the rotational starting point is defined as the position at which the b frame and the s frame are coincident.
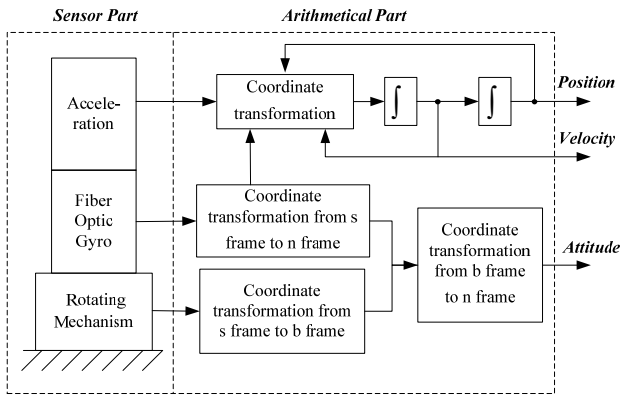
Fig. 1. A diagram of the navigation algorithm for the FOG INS rotation.

The rotational process in one modulation period is as follows:

Step 1: The IMU is rotated at $90°$ along the oz_s axis, stopping at position B; Step 2: The IMU is rotated at $180°$ along the oz_s axis, stopping at position D; Step 3: The IMU is rotated at $-90°$ along the oz_s axis, stopping at position C; and Step 4: The IMU is rotated at $-180°$ along the oz_s axis, stopping at position A.

The direction of positive rotation is defined as clockwise. In the normal state, the stay time at the stop position ranges from a few minutes to tens of minutes. Here, the stay time used is 800 seconds. The single-axis rotation rule is illustrated in Fig. 2.
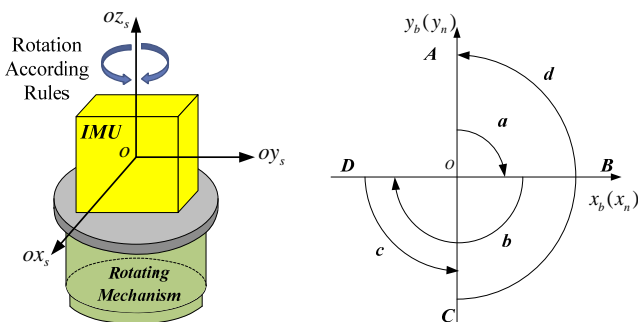

Fig. 2. The single-axis rotation rule.

In Fig. 2, x_i, y_i ($i = n, b$) represents the horizontal axis of the i coordinate system; a,b,c and d represent the rotation process; and A, B, C, and D represent the stay positions.

In single-axis rotation of the FOG INS, the analytical expression of the IMU error along the n frame is described as follows:

$$\begin{bmatrix} \varepsilon_x^{n(b)}(t) \\ \varepsilon_y^{n(b)}(t) \\ \varepsilon_z^{n(b)}(t) \end{bmatrix} = \begin{bmatrix} \varepsilon_x^s \cos \omega_0 t - \varepsilon_y^s \sin \omega_0 t \\ \varepsilon_x^s \sin \omega_0 t + \varepsilon_y^s \cos \omega_0 t \\ \varepsilon_z^s \end{bmatrix} \quad (1)$$

where ε_j^i ($i = n, b$, $j = x, y, z$) represents the FOG error projected along the j axis of the i coordinate system, ω_0 represents the rotational angular velocity ($\omega_0 \neq 0$ during rotation; $\omega_0 = 0$ at the stay position), and t represents the rotation time in process a-d.

From equation (1), it can be seen that in the process of rotating, $\omega_0 \neq 0$, and the IMU error along the horizontal axis of the n coordinate systems is a periodic quantity following the sine and cosine. Additionally, in the process of staying, $\omega_0 = 0$, and the IMU error along ε_{xy}^n, ε_{yx}^n and ε_{yy}^n is opposite at the coupled opposite positions, which have a difference of $180°$.

III. ATTITUDE ERROR ANALYSIS FOR THE FOG INS ROTATION

A. Modulation form of the FOG error

Combining the rotation rules in Fig. 2 and the IMU error along the n coordinate system as equation (1), the modulation form of the FOG error along the horizontal axis of the n coordinate system in one modulation period is shown in Fig. 3.
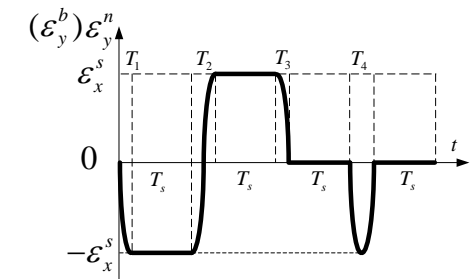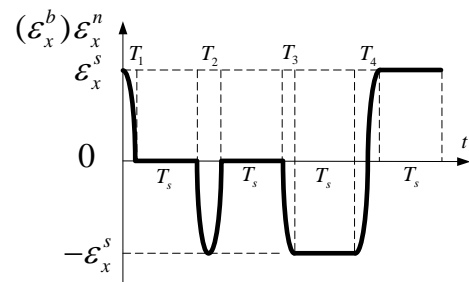
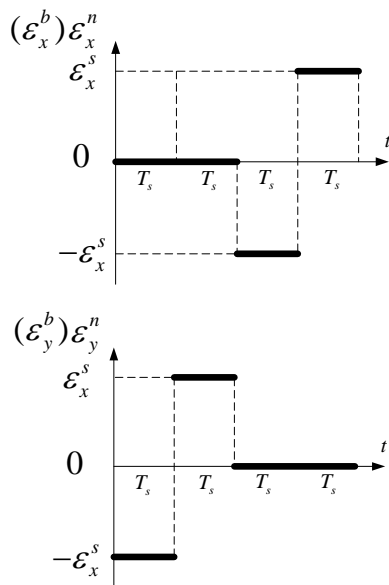(a) The modulation form of ε_x^s along the horizontal axis
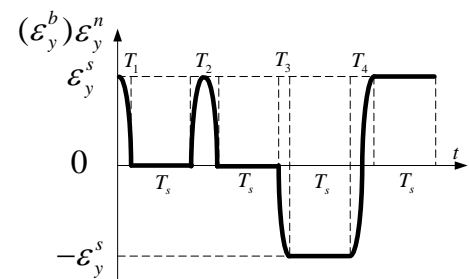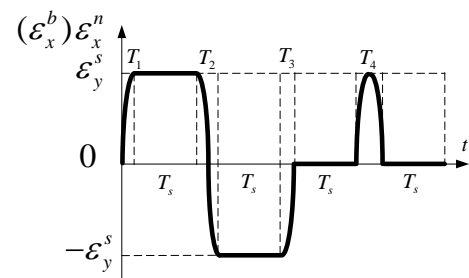
(b) The modulation form of ε_y^s along the horizontal axis

Fig. 3. The modulation form of the FOG error along the horizontal axis of the n coordinate system.

In Fig. 3, T_s represents the stay time, and $T_s = 800$ s. Additionally, T_k ($k = 1, 2, 3, 4$) represents the time of rotation as rotation progresses, and the rotation velocity is set as $\omega_0 = 6° / s$; therefore, $T_1 = T_3 = 15s$ and $T_2 = T_4 = 30s$.

In comparison to the stay time T_s , the rotation time T_k is very short. Hence, the rotational process can be neglected during one modulation period. The modulation form of the FOG error along the horizontal axis of the n coordinate system in one modulation period changes as illustrated in Fig. 4.

Therefore, in one period of single-axis rotation modulation, the rotational characteristics of the horizontal FOG along the n coordinate system appears to be a periodic function, as illustrated in Fig. 4, with a rotational period of $T = 4T_s = 3200s$.

(a) The modulation form of ε_x^s along the horizontal axis after simplification
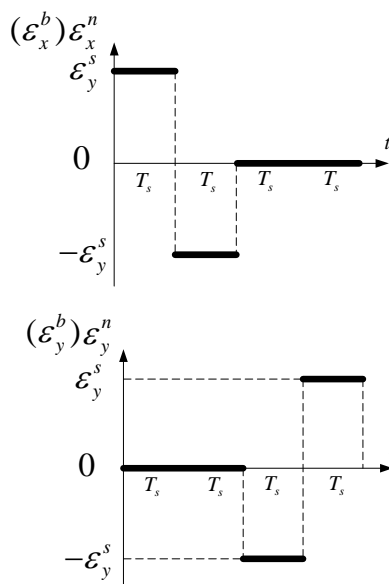
(b) The modulation form of ε_y^s along the horizontal axis after simplification

Fig. 4. The modulation form of the FOG error along the horizontal axis of the n coordinate system after simplification.

B. Fourier series expansion for the FOG error

Based on the principles of Fourier series, which are used to develop periodic functions, in satisfying the following conditions, the error can be expanded as a periodic function. (1) The periodic functions have a finite number of discontinuous points. (2) The periodic functions have a finite number of extreme points. This means that periodic functions can be expanded as a sum of sine and cosine functions.

For example, the modulated form of the FOG error ε_x^s along the ox_n axis of the n coordinate system is described as

$$\varepsilon_{xx}^n (t) = \begin{cases} 0 & (0 < t \leq T/4) \\ 0 & (T/4 < t \leq T/2) \\ -\varepsilon_x^s & (T/2 < t \leq 3T/4) \\ \varepsilon_x^s & (3T/4 < t \leq T) \end{cases} \quad (2)$$

where ε_{xx}^n represents the projected result along the ox_n axis, which is caused by the FOG error of the ox_s axis.

This yields the $\varepsilon_{xx}^n(t)$ Fourier series expansion

$$\varepsilon_{xx}^n (t) = \frac{a_0}{2} + \sum_{n=1}^{\infty} \left(a_n \cos n\omega t + b_n \sin n\omega t \right) \quad (3)$$

where,

$$\begin{cases} a_n = \frac{2}{T} \int_{-\frac{T}{2}}^{\frac{T}{2}} f_T (t) \cos n\omega t dt & (n = 0, 1, 2, \cdots) \\ b_n = \frac{2}{T} \int_{-\frac{T}{2}}^{\frac{T}{2}} f_T (t) \sin n\omega t dt & (n = 1, 2, 3, \cdots) \end{cases} \quad (4)$$

where $f_T(t) = \varepsilon_{xx}^n (t)$.

Substituting equation (2) into equation (4),

$$\begin{cases} a_0 = 0 \\ a_n = \frac{2\varepsilon_x^s}{n\pi} \sin \frac{n\pi}{2} \left(1 - \cos \frac{n\pi}{2} \right) & (n = 1, 2, 3, \cdots) \\ b_n = \frac{2\varepsilon_x^s}{n\pi} \cos \frac{n\pi}{2} \left(1 - \cos \frac{n\pi}{2} \right) & (n = 1, 2, 3, \cdots) \end{cases} \quad (5)$$

Substituting equation (5) into equation (3),

$$\varepsilon_{xx}^n (t) = \sum_{n=1}^{\infty} \left[\frac{2\varepsilon_x^s}{n\pi} \sin \frac{n\pi}{2} \left(1 - \cos \frac{n\pi}{2} \right) \cos n\omega t + \frac{2\varepsilon_x^s}{n\pi} \cos \frac{n\pi}{2} \left(1 - \cos \frac{n\pi}{2} \right) \sin n\omega t \right] \quad (6)$$

Similarly, the projected result of $\varepsilon_{xy}^n(t)$ ($\varepsilon_{yx}^n(t)$, $\varepsilon_{yy}^n(t)$) along the ox_n (oy_n) axis, as caused by the FOG error of the oy_s (ox_s) axis, can be obtained as follows:

$$\varepsilon_{xy}^n (t) = \sum_{n=1}^{\infty} \left[\frac{2\varepsilon_x^s}{n\pi} \sin \frac{n\pi}{2} \left(-1 + \cos \frac{n\pi}{2} \right) \cos n\omega t + \frac{2\varepsilon_x^s}{n\pi} \cos \frac{n\pi}{2} \left(1 - \cos \frac{n\pi}{2} \right) \sin n\omega t \right] \quad (7)$$

$$\varepsilon_{yx}^n(t) = \sum_{n=1}^{\infty}\left[\frac{2\varepsilon_y^s}{n\pi}\sin\frac{n\pi}{2}\left(1-\cos\frac{n\pi}{2}\right)\cos n\omega t + \right.$$
$$\left. \frac{2\varepsilon_y^s}{n\pi}\cos\frac{n\pi}{2}\left(-1+\cos\frac{n\pi}{2}\right)\sin n\omega t\right] \quad (8)$$

$$\varepsilon_{yy}^n(t) = \sum_{n=1}^{\infty}\left[\frac{2\varepsilon_y^s}{n\pi}\sin\frac{n\pi}{2}\left(1-\cos\frac{n\pi}{2}\right)\cos n\omega t + \right.$$
$$\left. \frac{2\varepsilon_y^s}{n\pi}\cos\frac{n\pi}{2}\left(1-\cos\frac{n\pi}{2}\right)\sin n\omega t\right] \quad (9)$$

where ε_{ij}^n ($i,j=x,y$) represents the projected result along the oi_n axis, which is caused by the FOG error of the oj_s axis.

C. Attitude error equation of the FOG INS rotation

In FOG INS rotation, IMU is placed on a turntable, and it is rotated on the turntable around one rotation axis according to established rules. Hence, the error equation of FOG INS rotation along frame n is shown as follows

$$\begin{cases} \delta\dot{v}_x = -\beta g + \Delta A_x^n \\ \delta\dot{v}_y = \alpha g + \Delta A_y^n \\ \dot{\alpha} = -\delta v_y / R + \beta\Omega\sin\varphi - \gamma\Omega\cos\varphi + \varepsilon_x^n \\ \dot{\beta} = \delta v_x / R - (\alpha+\delta\varphi)\Omega\sin\varphi + \varepsilon_y^n \\ \dot{\gamma} = \delta v_x \tan\varphi / R + (\alpha+\delta\varphi)\Omega\cos\varphi + \varepsilon_z^n \\ \delta\dot{\varphi} = \delta v_y / R \\ \delta\dot{\lambda} = \delta v_x \sec\varphi / R \end{cases} \quad (10)$$

where α, β, and γ represent the misalignment angles of pitch, roll, and heading, which reflect the accuracy of FOG INS rotation calculating attitude. The shorter the misalignment angles are, the better the attitude accuracy is. δv_l ($l=x,y$) represents calculating velocity error of FOG INS rotation; $\delta\varphi$, $\delta\lambda$ are latitude and longitude error calculated by rotation FOG INS; Ω represents the angular velocity of Earth's rotation, R represents earth radius; φ represents the latitude of the vehicle; ΔA_l^n ($l=x,y$) represents accelerometer error along l axis of n frame.
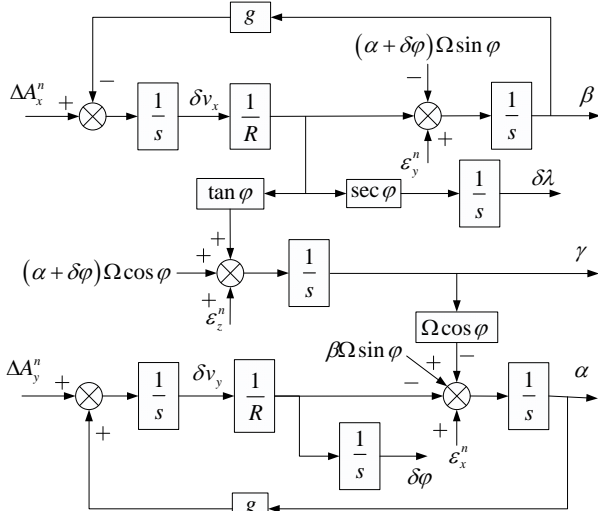

Fig. 5. Diagram of rotation FOG INS error.

Based on equation (10), the diagram of system error is shown in Fig. 5.

In Fig. 5, the system input signal of ΔA_x^n, ΔA_y^n, ε_x^n, ε_y^n, ε_z^n is changed in FOG INS rotation. Combining equation (11) and Fig. 5, the relationship between misalignment angles and the FOG error is described as follows:

$$\begin{bmatrix}\alpha(s)\\\beta(s)\\\gamma(s)\end{bmatrix} = \begin{bmatrix}\dfrac{s^3}{\Delta_0(s)} & \dfrac{\omega_{iez}s^2}{\Delta_0(s)} & \dfrac{-\omega_{iey}s^2}{\Delta_0(s)} \\[2mm] \dfrac{-\omega_{iez}s^2}{\Delta_0(s)} & \dfrac{s(s^2+\omega_{iey}^2)}{\Delta_0(s)} & \dfrac{\omega_{iey}\omega_{iez}}{\Delta_0(s)} \\[2mm] \dfrac{M_1}{\Delta_0(s)} & \dfrac{M_2}{\Delta_0(s)} & \dfrac{M_3}{\Delta_0(s)}\end{bmatrix}\begin{bmatrix}\varepsilon_{xx}^n(s)+\varepsilon_{xy}^n(s)\\\varepsilon_{yx}^n(s)+\varepsilon_{yy}^n(s)\\\varepsilon_z^n(s)\end{bmatrix}$$

$$(11)$$

where, $\omega_{iez}=\Omega\sin\varphi$, $\omega_{iey}=\Omega\cos\varphi$, $M_1=\left(\omega_{iey}s^2+\Omega\omega_s^2\sec\varphi\right)$, $M_2=s\tan\varphi\left(\omega_{iey}^2-\omega_s^2\right)$, $M_3=s\left(s^2+\omega_s^2+\omega_{iez}^2\right)$, $\Delta_0(s)=\left(s^2+\omega_s^2\right)\left(s^2+\Omega^2\right)$, $\omega_s=\sqrt{g/R}$ represents the Schuler frequency;

We take the relationship between $\varepsilon_{xx}^n(s)$ and the misalignment angles as an example. After being combined with equation (6) and using the Laplace transformation of $\varepsilon_{xx}^n(t)$, $\varepsilon_{xx}^n(s)$ can be obtained as

$$\varepsilon_{xx}^n(s) = \frac{2\varepsilon_x^s}{\pi}\left(\underbrace{\frac{s}{s^2+\omega^2}}_{n=1} - \underbrace{\frac{2\omega}{s^2+4\omega^2}}_{n=2} - \underbrace{\frac{s/3}{s^2+9\omega^2}}_{n=3} + \underbrace{\cdots}_{n=4,5,\cdots}\right) \quad (12)$$

Substituting (12) into (6), the relationships between $\varepsilon_{xx}^n(s)$ and the misalignment angles are

$$\begin{cases} \alpha(s) = \dfrac{2\varepsilon_x^s}{\pi}\dfrac{s^3}{\Delta_0(s)}\left(\dfrac{s}{s^2+\omega^2}-\dfrac{2\omega}{s^2+4\omega^2}-\dfrac{s/3}{s^2+9\omega^2}+\cdots\right) \\[3mm] \beta(s) = -\dfrac{2\varepsilon_x^s}{\pi}\dfrac{\omega_{iez}s^2}{\Delta_0(s)}\left(\dfrac{s}{s^2+\omega^2}-\dfrac{2\omega}{s^2+4\omega^2}-\dfrac{s/3}{s^2+9\omega^2}+\cdots\right) \\[3mm] \gamma(s) = \dfrac{2\varepsilon_x^s}{\pi}\dfrac{\Omega(\cos\varphi s^2+\omega_s^2\sec\varphi)}{\Delta_0(s)}\left(\dfrac{s}{s^2+\omega^2}-\dfrac{2\omega}{s^2+4\omega^2}-\right. \\[3mm] \qquad\left.\dfrac{s/3}{s^2+9\omega^2}+\cdots\right) \end{cases}$$

$$(13)$$

In observing equation (13), the misalignment angles can be identified to possess the frequency of Schuler and Earth periodicities. Additionally, a new type of concussion error is introduced to the misalignment angles that is related to the frequency of ω, 2ω, $3\omega\cdots$, and the amplitude of oscillation is decreased with the growth in frequency. This conclusion is also suitable for discerning the effect of ε_{xy}^n, ε_{yx}^n, and ε_{yy}^n on the misalignment angles.

In short, in the single-axis FOG INS rotation, the FOG error, which occurs along the horizontal axis of the n coordinate system, is the sum of the sine and cosine with different frequencies of ω, 2ω, $3\omega\cdots$. Additionally, the misalignment angles are affected by the FOG error; that is, the form of the misalignment angles oscillates with the sum of the sine and cosine and possesses a frequency that

corresponds to that of the Schuler and Earth periods, ω, 2ω, 3ω $\cdots$. The azimuthal FOG error ε_z^n along the rotating shaft is not modulated. Therefore, only the Schuler and Earth period errors are incorporated into the misalignment angles by ε_z^n.

IV. ATTITUDE ERROR MITIGATION APPROACH FOR THE FOG INS ROTATION

A. The principles of attitude error mitigation

To simplify the analyzing problem, the coupling terms of $\delta v_x \tan\varphi / R$ and other symbols between level misalignments angles, angular velocity of earth rotation are ignored in Fig. 5, because they are driblet. And the position error channels are also omitted. Then the diagram of rotation FOG INS error is separated into two parts, which is shown in Fig. 6.
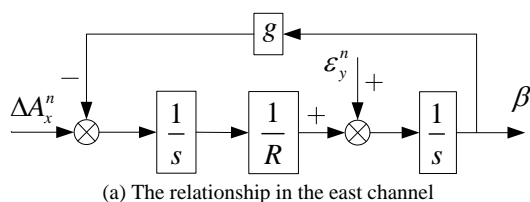
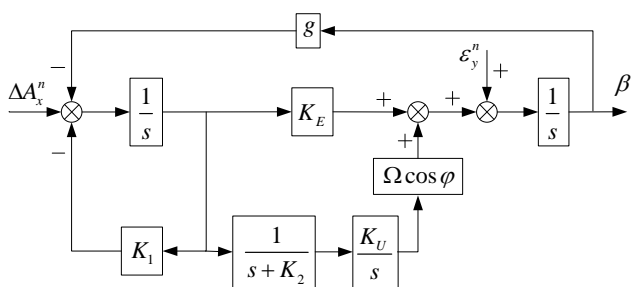(a) The relationship in the east channel
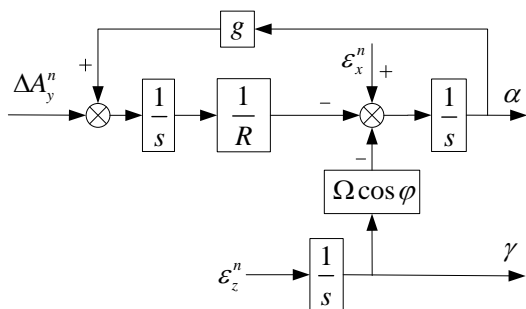
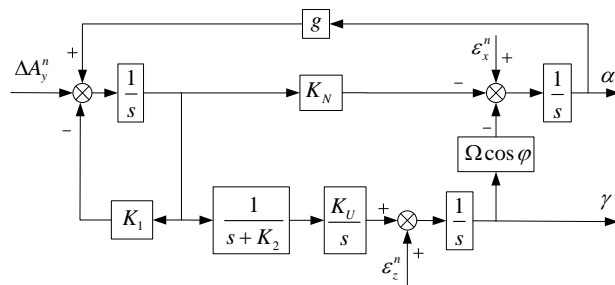(b) The relationship in the north and azimuth channels
Fig. 6. A diagram of the relationship between the IMU error and the misalignment angles.

In Fig. 6, ΔA_l^n ($l = x, y$) represents the accelerometer error along the l axis of the n frame.

In Fig. 6, the characteristic equation is $\Delta(s) = s^2 + \omega_s^2$, and $\omega_s = \sqrt{g/R}$. Therefore, the system outputs of α, β, and γ are unstable, oscillating with a frequency of ω_s. To eliminate the oscillation, a group of navigational parameters is introduced into the calculation process. An equivalent transformation of the relationship between the IMU error and the misalignment angles is shown in Fig. 7.

(a) The relationship in the east channel

(b) The relationship in the north and azimuth channels
Fig. 7. A diagram of the navigational parameters.

In Fig. 7, K_1, K_2, K_E, K_N, and K_U are the navigational parameters. The damping term is introduced to the system by the navigational parameter K_1. The natural period is shortened by introducing the navigational parameter K_2; the effects of K_E, K_N, and K_U are energy storage; and the parameter of $1/R$ is included in K_E and K_N.

We take the relationship between ε_x^n and γ as an example; then, the transfer function can be described as

$$\gamma(s) = \frac{gK_U \cdot \varepsilon_x^n(s)}{s^2(s+K_1)(s+K_2) + s(s+K_2)K_N g + K_U g \omega_{iey}} \quad (14)$$

Next, let the characteristic root be $s_{1,2} = -\xi\omega_n$, $s_{3,4} = -\xi\omega_n + j\sqrt{1-\xi^2}\omega_n$, where ξ is the damping coefficient and ω_n is the natural frequency. Equation (14) can be described as

$$\gamma(s) = \frac{\xi^2 \omega_n^4}{\Omega\cos\varphi} \cdot \frac{1}{(s^2 + 2\xi\omega_n s + \omega_n^2)(s+\xi\omega_n)^2} \varepsilon_y^n(s) \quad (15)$$

where $K_1 = K_2 = 2\xi\omega_n$, $K_E = K_N = \omega_n^2(1+\xi^2)/g$, and $K_U = \xi^2\omega_n^4 / \Omega\cos\varphi g$.

From equation (15), the following conclusions can be drawn: as long as the navigational parameters of ξ and ω_n are reasonably established, the system is stable. That is, the system outputs of α, β, and γ are stable by introducing K_1, K_2, K_E, K_N, and K_U into the calculation process.

Based on equation (15), the amplitude-frequency curve between ε_x^n and γ is shown in Fig. 8. To obtain a unique curve, $\xi = 0.707$.
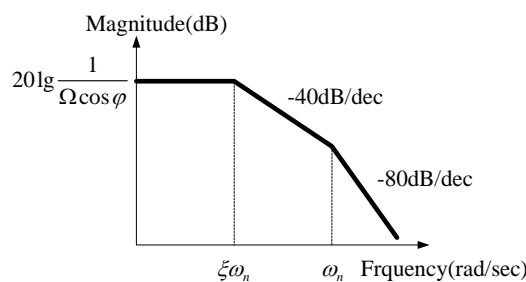
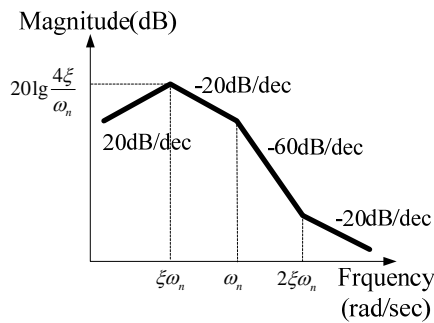Fig. 8. The amplitude-frequency curve between ε_x^n and γ.

From Fig. 8, we can see that the effect of ε_x^n on γ is a low-pass in the frequency domain. The input signal, which possesses a frequency higher than $\xi\omega_n$, will be an inhibition

in the system. Additionally, the inhibition increases with the input signal frequency. Based on the conclusion presented in section 3, the FOG error, which exists along the horizontal axis of the n frame, is the sum of sine and cosine functions with different frequencies of ω, 2ω, 3ω $\cdots$. Therefore, if ξ and ω_n are adjusted appropriately and reach the target of $\xi\omega_n < \omega$, the effect of the FOG error with a frequency of ω, 2ω, 3ω $\cdots$ on γ can be inhibited. Additionally, because $\omega > \omega_s > \Omega$, a value of γ with the frequency of the Schuler and Earth periods also can be inhibited with the same ξ and ω_n.

Based on Fig. 8, the amplitude-frequency curves between ε_x^n and α and between ε_y^n and β are shown in Fig. 9. These curves were developed according to the same method.
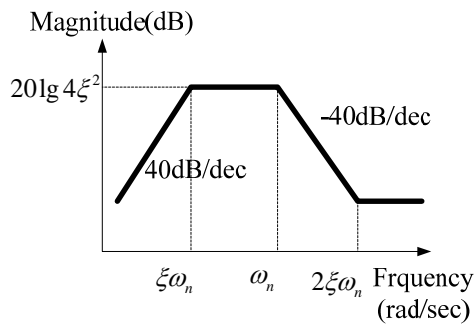
(a) The amplitude-frequency curves between ε_x^n and α

(b) The amplitude-frequency curves between ε_y^n and β

Fig. 9. The amplitude-frequency curves.

From Fig. 9, the gains in the system output are $20\lg 4\xi^2$ and $20\lg(4\xi/\omega_n)$ based on ε_x^n and ε_y^n. The design principle of ω_n is $\omega_n \ll 1$, so $20\lg 4\xi^2 \ll 20\lg(4\xi/\omega_n)$. If the effect of ε_y^n on β can be inhibited with a group of ξ and ω_n, the gain of α caused by ε_x^n is small.

Comparing the amplitude-frequency curve in Fig. 9(b) with that in Fig. 8, it can be seen that the curves in these two figures are similar to each other and that the effect on the misalignment angles of the input signal with a frequency higher than $\xi\omega_n$ can be inhibited. Therefore, if the effect of ε_x^n on γ can be inhibited with a group of ξ and ω_n, the effect of ε_y^n on β can also be inhibited.

B. Design principle of the attitude error parameters

We take the relationship between ε_x^n and γ as an example. Accordingly, the design principle of the attitude error parameters is derived to inhibit the new type of concussion attitude error obtained, which is related to the rotational period. Based on equation (15) and Fig. 8, when the frequency of the input signal is $\omega > \omega_n$, an amplification of the azimuth misalignment angle is obtained:

$$M_{\varepsilon_y^n}^{\gamma}(\omega) = \frac{\xi^2 \omega_n^4}{\omega^4 \Omega \cos\varphi} \quad (\omega > \omega_n) \tag{16}$$

where $M_{\varepsilon_x^n}^{\gamma}$ represents the amplification of γ caused by ε_y^n.

In the single-axis FOG INS rotation, the FOG error along the horizontal axis of the n coordinate system is the sum of sine and cosine functions with different frequencies of ω, 2ω, 3ω $\cdots$. Additionally, the FOG error is the input signal of the system. Based on (16), the following conclusion can be obtained: in the case in which ω is a fixed value and the principle of $\omega_n < \omega$ is satisfied, the amplification of $M_{\varepsilon_x^n}^{\gamma}(\omega)$ at the frequency of ω is smaller than under steady amplification. Further, the effect of the FOG error on the misalignment angles can be inhibited. In particular, the inhibitory effect increases with the input signal frequency.

To further improve the inhibitory effect and decrease the attitude error, the value of ω_n should be set significantly smaller. When the effect of ε_x^n on the azimuth misalignment angles is decreased n times, the relationship between $M_{\varepsilon_x^n}^{\gamma}(\omega)$ and ω should be satisfied:

$$M_{\varepsilon_y^n}^{\gamma}(\omega) = \frac{\xi^2 \omega_n^4}{\omega^4 \Omega \cos\varphi} \leq \frac{1}{n\Omega \cos\varphi} \tag{17}$$

Solving the inequality, the equation of ω_n can be obtained as follows

$$\omega_n \leq \omega \cdot \sqrt[4]{1/(n\xi^2)} \tag{18}$$

The design principle of the attitude error parameters is shown in equation (18), and the conclusion is also used for the design principle of β (or α) caused by ε_y^n (or ε_x^n). Hence, the attitude accuracy can be improved by introducing the parameters ξ and ω_n in the calculation process for FOG INS rotation.

V. SIMULATION ANALYSIS AND THE EXPERIMENTAL STUDY

A. Simulation Analysis

According to the above analysis, we performed a MATLAB simulation under the following conditions:

a) The constant drift of the FOG is $0.01°/h$. The scale factor error of the FOG is 1×10^{-5}. The measurement noise of the FOG is Gaussian white noise with an amplitude of $0.001°/h$, and the accelerometer bias is $10^{-4}g$.

b) The latitude is $45.7796°N$, and the longitude is $126.6709°E$.

c) The rotation rules for the FOG INS are shown in Fig. 2. The rotation angle velocity is $\omega_0 = 6^\circ / s$, and the stay time at each position is $800s$. Hence, one rotational period is $T \approx 3200s$, and $\omega = 2\pi / T = 0.00196 rad / s$.

d) Combined with equation (18), $n = 50$ and $\xi = 0.707$, so $\omega_n \leq 8.8824 \times 10^{-4}$. Setting $\omega_n = 5.0 \times 10^{-4}$, then $K_1 = K_2 = 2.828 \times 10^{-4}$, $K_E = K_N = 6.1218 \times 10^{-9}$, and $K_U = 7.8264 \times 10^{-13}$ are further calculated.

e) The sampling interval is $0.01s$, and the simulation time is 48 hours.
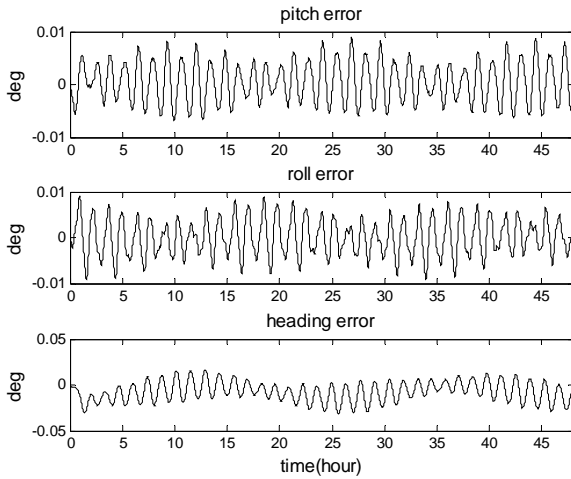
(a) The misalignment angles without setting the parameters
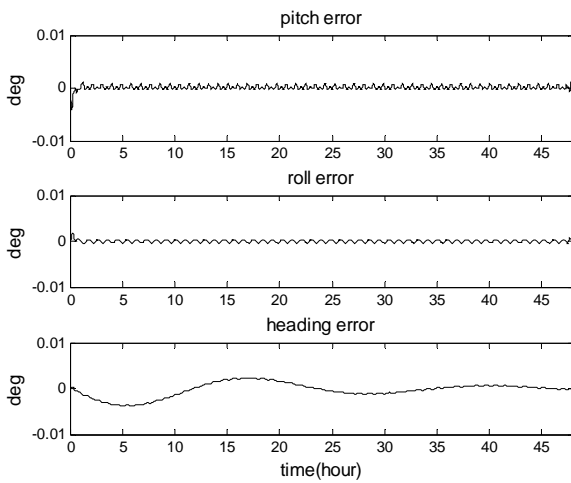
(b) The misalignment angles with parameters ξ and ω_n

Fig. 10. The misalignment angles for single-axis FOG INS rotation.

Fig. 10 presents the misalignment angles for a single-axis FOG INS rotation: Fig. 10(a) depicts the misalignment angles without setting the parameters, while Fig. 10(b) shows the misalignment angles with the parameters of ξ and ω_n, which are set as the simulation conditions specified in above item d).

From Fig. 10, the following conclusion can be obtained: the misalignment angles can be decreased by introducing the parameters ξ and ω_n in the attitude calculation.

B. Experimental Study

To validate the method of decreasing the attitude error by introducing the parameters ξ and ω_n in the calculation process for the FOG INS rotation, an experiment was conducted by fixing the FOG INS in a rotating mechanism. The INS was rotated by the mechanism to different positions according to the rotation rules described in Fig. 2. The FOG INS was developed by our lab, and the performance index of the FOG and the 920E rotating mechanism are given in table I and table II. The IMU and the rotating mechanism are shown in Fig. 11.

Fig. 11. The FOG INS and the rotating mechanism.

TABLE I
THE FOG PERFORMANCE INDEX

| Parameter Item	Index
Dynamic Range	$\pm 100^\circ / s$
Bias Stability	$\leq 0.003^\circ / h$
Random Walk	$\leq 0.001^\circ / \sqrt{h}$
Nonlinear Degree of Scale Factor	$\leq 5 ppm$

TABLE II
THE MAIN PARAMETERS OF THE 920E

Parameter Item	Index
Requirements of load	A weight of 50 kg
Rotary precision of station	$\pm 2''$ with inner, middle, outer gimbal
Rotation range of station	Continuous and infinite
Working mode	Idle, location, rate, servo, rocking
Angle measurement accuracy	$\pm 3''$
Angle measurement repetition	$\pm 2''$
Position accuracy	$\pm 3''$
Rate range	$0.001 - 150^\circ / s$
Rate accuracy	5×10^{-5} (mean of 360°) 1×10^{-2} (mean of 1°)

In the experiment, the rotational starting point was defined as the position at which the b frame and the s frame differ by 325°. The process of rotation for one modulation period is as follows:

Step 1: The IMU is rotated by 90° along the oz_s axis, stopping at position B; Step 2: The IMU is rotated by 180° along the oz_s axis, stopping at position D; Step 3: The IMU is rotated by -90° along the oz_s axis, stopping at position C; and Step 4: The IMU is rotated by -180° along the oz_s axis, stopping at position A.

The direction of positive rotation was defined as clockwise, and the stay time used was 800 seconds. The rotation angle

velocity was set at $6°/s$. The parameters were the same as those used in the simulation. The experimental time was 48 hours. Fig. 12 shows the misalignment angles for the single-axis FOG INS rotation in the experiment: Fig. 12(a) presents the misalignment angles without setting the parameters, while Fig. 12(b) shows the misalignment angles with the ξ and ω_n parameters.
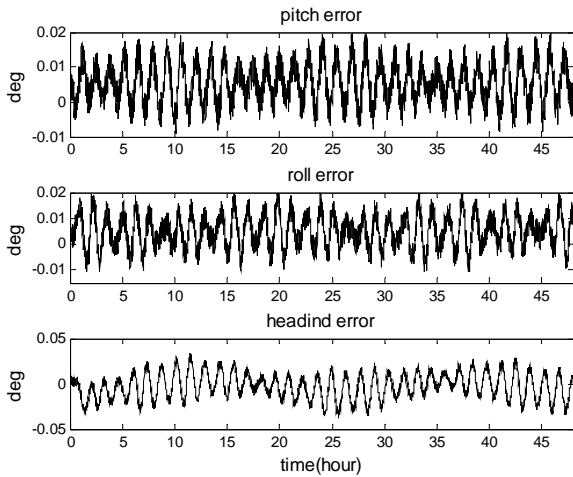
(a) The misalignment angles without setting the parameters
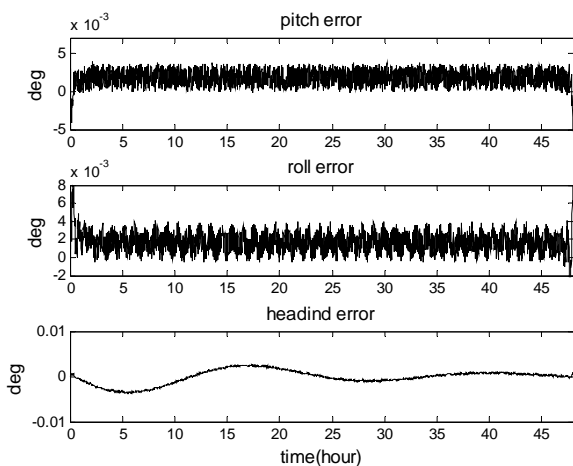
(b) The misalignment angles with the ξ and ω_n parameters

Fig. 12. The misalignment angles for the single-axis FOG INS rotation in the experiment.

Comparing the curves in Fig. 12(a) with those in Fig. 12(b), the attitude error, which possesses the frequency of the Schuler and Earth periods, ω, 2ω, 3ω $\cdots$, can be inhibited by introducing parameters ξ and ω_n into the experimental attitude calculations.

VI. CONCLUSION

According to single-axis FOG INS rotation, the form of the misalignment angles was analyzed in navigation calculations. The misalignment angles were developed with the frequency of Schuler and Earth periods. Additionally, a new type of concussion error was introduced, which was related to the frequency of $k\omega$ ($k=1,2,3\cdots$). Further, the oscillation amplitude was found to decrease with increasing frequency. An attitude error mitigation approach was proposed for FOG INS rotation based on the amplitude-frequency curves between the FOG error and the misalignment angles. It was found that the attitude error could be inhibited by introducing ξ and ω_n in the calculation process. The results of the simulation and experiment for the FOG INS demonstrated improved attitude accuracy.

REFERENCES

[1] Curey R K, Ash M E, Thielman L O, "Proposed IEEE inertial systems terminology standard and other inertial sensor standard," *IEEE Position Location Navigation Symposium. Temecula,* CA, USA: IEEE, pp. 83-90, 2004.
[2] Weston J L, Titterton D H, "Modern inertial navigation technology and its application," *Electronics and Communication Engineering Journal*, pp. 49-64, 2000(8).
[3] Broxmeyer C, "Damping an Inertial Navigation System in R.E Roberson and J.S Farrior," *Guidance and Control*. Academic Press Inc, New York, 1962.
[4] Chong-Moo Lee, Pan-Mook Lee, Seok-Won Hong, Sea-Moon Kim, Woojae Seong, "Underwater Navigation System Based on an Inertial Sensor and a Doppler Velocity Log Using Indirect Feedback Kalman Filter," Processing of the Fourteenth (2004) *International Offshore and Polar Engineering Conference*, pp. 214, 2004.
[5] ARTHUR GELB, "Synthesis of a Very Accurate Inertial Navigation System," *IEEE Transactions on Aerospace and Navigational Electronics*, pp. 119-128, 1965.
[6] CHENG Jianhua, ZHAO Lin, SONG Juncai, "Application of auto_compensation technology to the switches of INS states," *Journal of Harbin Engineering University*, 26(6): pp. 744-749, 2005.
[7] NASH R A, "The estimation and control of terrestrial INS error due to vertical deflections," *IEEE Transactions on Automatic Control*, 13(4), pp. 329-337, 1968.
[8] Lei Yuanchao, *Inertial navigation systems*, Beijing: National Defence Industry Press, 1978, pp. 89-96.
[9] Ishibashi S, Tsukioka S, Sawa T, et al, "The rotation control system to improve the accuracy of an inertial navigation system installed in an autonomous underwater vehicle," *Workshop on Scientific Use of Submarine Cables and Related Technologies 2007*, pp. 495-498, 2007.
[10] Terry T, Emanuel L, "The AN/WSN-7B Marine Gyrocompass / navigator," Proceedings of the *2000 National Technical Meeting of the Institute of Navigation*, 2000, pp. 348-357.
[11] Levinson E, Willcocks M, "The next generation marine inertial navigation is here now," *IEEE Position Location and Navigation Symposium*, 1994, pp. 121-127.
[12] Ben Yueyang, Sun Feng, Gao Wei, et al, "Generalized Method for Improved Coning Algorithms using Angular Rate," 2011 *IEEE Transactions on Aerospace and Electronic Systems*, pp. 1565-1572, 2009.
[13] ZHANG ling, LIU Jian-ye, LAI Jizhou, "Rotating fiber optic gyro strap-down inertial navigation system with three rotating axes," *Transaction of Nanjing University of Aeronautics & Astronautics,* 25(4): pp. 289-294, 2008.
[14] Gao Wei, Ben Yueyang, Zhang Xin, et al, "Rapid Fine Strapdown INS Alignment Method under Marine Mooring Condition," 2011 *IEEE Transactions on Aerospace and Electronic Systems*, pp. 2887-2896, 2011.
[15] LIU Wen-ren, TANG Yan, ZHU Lei, "Effects of MINS rotation-modulating on transfer alignment," *Journal of Chinese Inertial Technology*, 19(1): pp. 16-20, 2011.
[16] Miller P A, Farrell J A, Yuanyuan Z, et al, "Autonomous Underwater Vehicle Navigation," *IEEE Journal of Oceanic Engineering*, 35(3): pp. 663-678, 2010.
[17] SUN Feng, SUN Wei, GUO Zhen, "Auto-compensation method of SINS based on IMU rotation," *Chinese Journal of Scientific Instrument*, 30(12): pp. 2511-2517, 2009.
[18] BAI Yanping, LEI Yingjie, YANG Ming, *Complex Function and Integral Transform*. Beijing: defense industry Press, 2006, pp. 166-167.
[19] HUANG Deming, CHENG Lu. *Inertial navigation systems*. Harbin: Harbin Engineering University Press, 1999, pp. 77-78.
[20] LI Bingjun, "*Research on Initial Alignment Technology for Strap-down Compass System Based on FOG*," Ph.D. dissertation, Harbin Engineering University. 2008, pp. 60-61.

[21] S. Strano, M. Terzo, "A First Order Model Based Control of a Hydraulic Seismic Isolator Test Rig," *Engineering Letters*, vol. 21, no. 2, pp. 52-60, May. 2013.

[22] Keiichi Tamura, Hajime Kitakami, Akihiro Nakada, "Distributed Modified Extremal Optimization using Island Model for Reducing Crossovers in Reconciliation Graph," *Engineering Letters*, vol. 21, no. 2, pp. 81-88, May. 2013.

[23] Louis Angelo Danao, Jonathan Edwards, Okeoghene Eboibi, Robert Howell, "A Numerical Investigation into the Effects of Fluctuating Wind on the Performance of a Small Scale Vertical Axis Wind Turbine," *Engineering Letters*, vol. 21, no. 3, pp. 149-157, August. 2013.

Zhao Qi is a PhD candidate in navigation, guidance and control at Harbin Engineering University. He received his bachelor degree from Harbin Engineering University in 2009. His research interests are in the areas of integrated navigation system, information fusion technology,etc.

Qiuying Wang is a PhD candidate in Precision Instrument and Machinery at Harbin Engineering University. She received her bachelor degree from Harbin Engineering University in 2009. Her research interests are in the areas of rotation fiber optic gyro strap-down inertial navigation, inertial alignment for strap-down inertial navigation, etc.